Supplementary material

Supplementary figure S1: Proximal convoluted tubule characterization.

Supplementary figure S2: Expression of markers in proximal tubule micro-dissected segments.

Supplementary figure S3: Endo-lysosomal protein expression along the proximal convoluted tubule.

Supplementary figure S4: Low molecular weight protein reabsorption in the proximal tubule

Supplementary figure S5: Comparison of free dye and labeled-albumin uptake

Supplementary table 1: Sequences of primers and efficiency of RT-PCR reactions.

Supplementary movie 1: Lysozyme and dextran uptake in the entire cortex of a cleared kidney.

Supplementary movie 2: 3D structure of proximal tubules in cleared cortex following lysozyme uptake

A

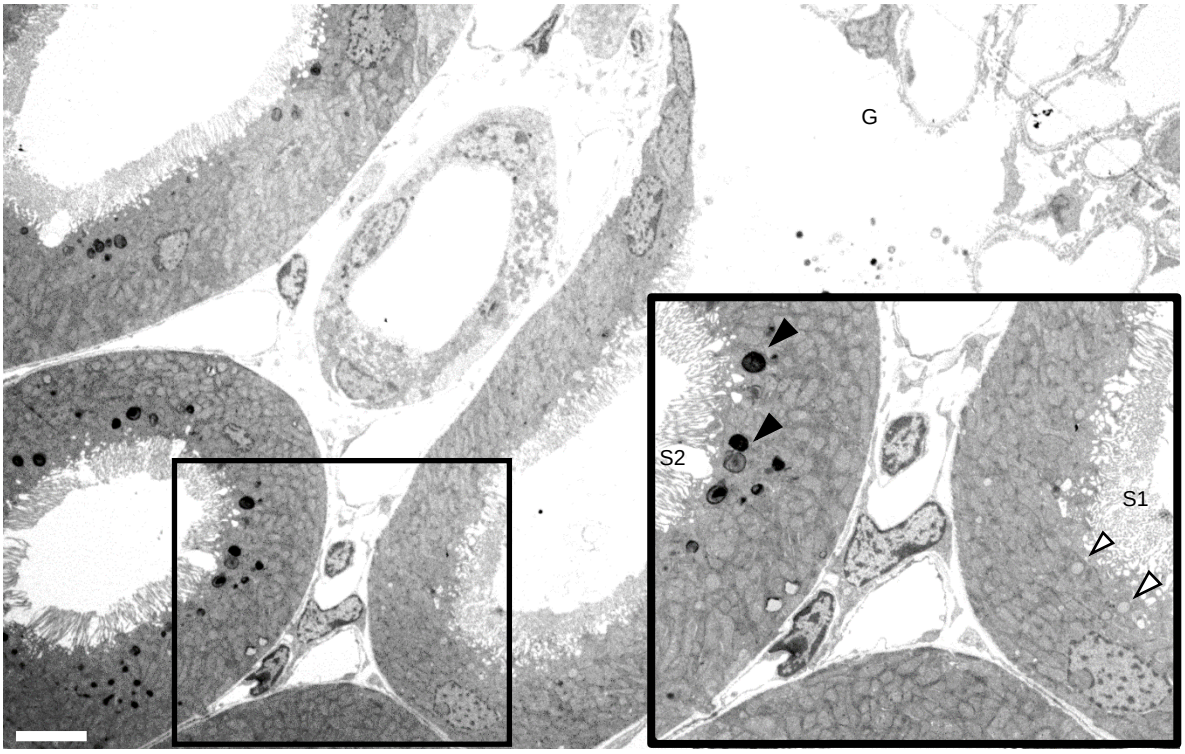

B

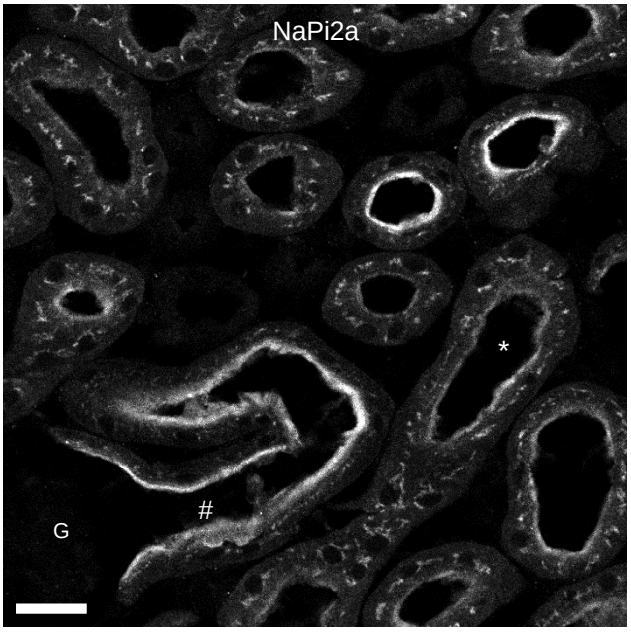

Figure S1: Proximal convoluted tubule characterization. (A) Transmission electron micrographs of S1 and S2 segments of the proximal tubule in the mouse kidney, showing differences in ultrastructure. S1 segments can be identified directly leaving the glomerulus (G), and contain electron lucent apical vacuoles (white arrowheads). In contrast, lysosomes in S2 segments are electron dense (black arrowheads). Scale bar: 5µm. (B) Tissue cryo-sections from mouse kidney cortex stained for the sodium-phosphate cotransporter NaPi2a in proximal convoluted tubules, revealing that expression levels are far higher in early (#) than late segments (*). The identity of early segments was confirmed by their emergence from glomeruli (G). Scale bar: 20µm.

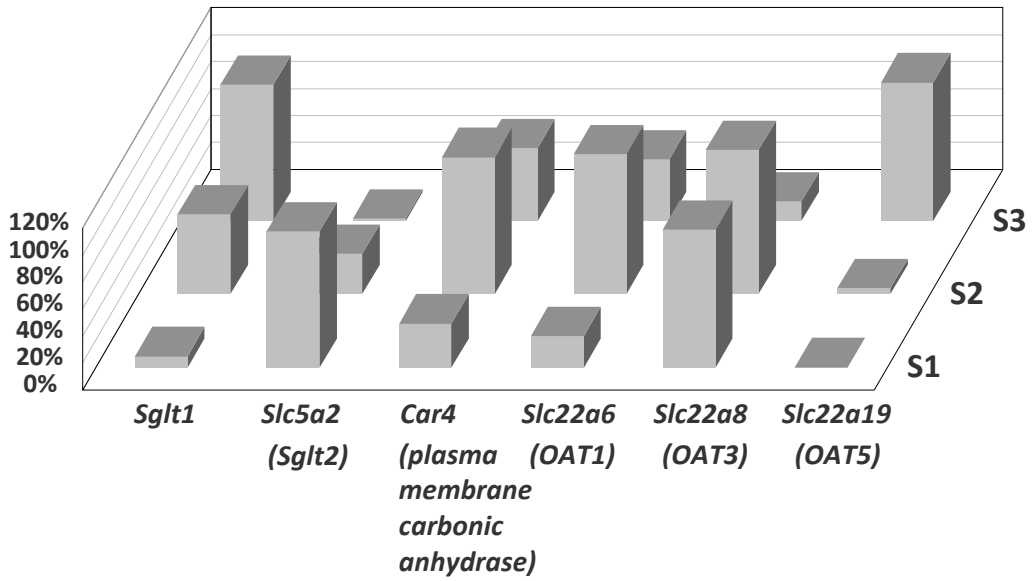

Figure S2: Expression of markers in proximal tubule micro-dissected segments. Segment-specific marker genes (S1: Slc5a2; S2: Car4; S3: Slc22a19) were used to demonstrate the purity for each fraction of collected tubules segments, using SYBR-green quantitative PCR. Quantification of all segment-specific marker genes was performed in comparison with GAPDH as an endogenous control. (n=8 S1, n=7 S2-S3).

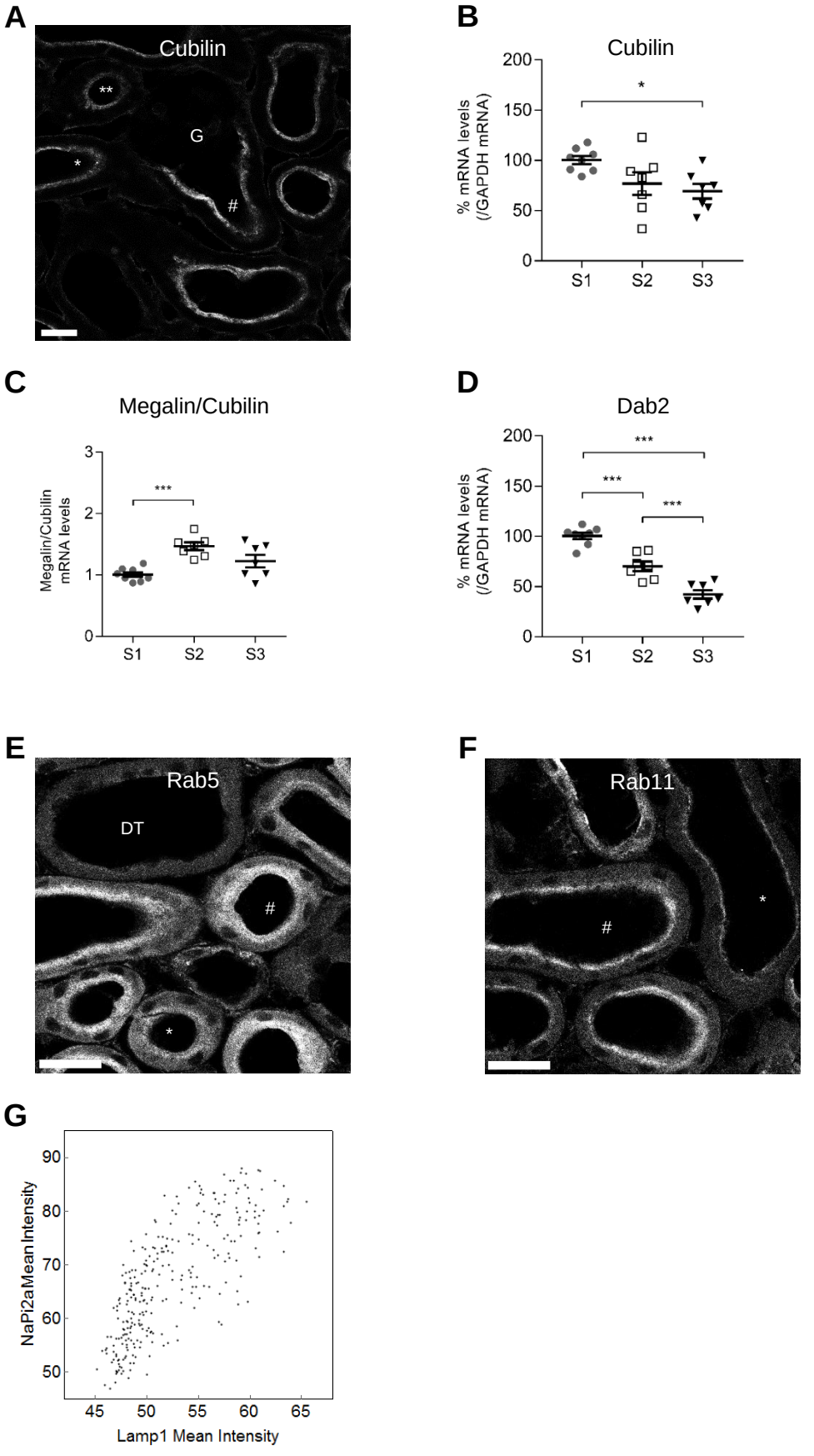
A
Cubilin
**
G
*
#
B
Cubilin
% mRNA levels (/GAPDH mRNA)
200
150
100
50
0
*
S1
S2
S3
C
Megalin/Cubilin
Megalin/Cubilin mRNA levels
3
2
1
0
***
S1
S2
S3
D
Dab2
% mRNA levels (/GAPDH mRNA)
200
150
100
50
0
***
***
***
S1
S2
S3
E
Rab5
DT
#
*
F
Rab11
*
#
G
NaPi2aMean Intensity
90
80
70
60
50
45
50
55
60
65
Lamp1 Mean Intensity

Figure S3: Endo-lysosomal protein expression along the proximal convoluted tubule. (A) Antibody staining of mouse kidney cortex showed that cubilin was expressed in both early (#) and late (*) proximal convoluted tubule segments. However, expression levels in S2 were highly variable, and a sub-section of S2 segments (**) showed markedly decreased fluorescence intensity. (B) RNA expression levels for cubilin decreased overall from S1 to S3 in micro-dissected segments, but also confirmed that expression was highly variable in S2 segments (*$p<0.05$). (C) Within individual nephrons, megalin/cubilin RNA expression ratio was significantly increased in S2 compared to S1 (***$p<0.001$). (D) RNA expression levels for the adaptor protein Disabled-2 (Dab2) decreased linearly along the proximal tubule (***$p<0.001$). (E-F) Protein expression levels of the early endosome marker Rab5 and recycling endosome marker Rab11 were both higher in early (#) than in late (*) proximal convoluted tubule segments. (G) The Lamp1 signal intensity within regions of interest drawn around sections of proximal convoluted tubules correlated positively with that of NaPi2a ($R=0.76$; $p<0.001$). Scale bars: 20μm. G: glomerulus. DT: distal tubule.

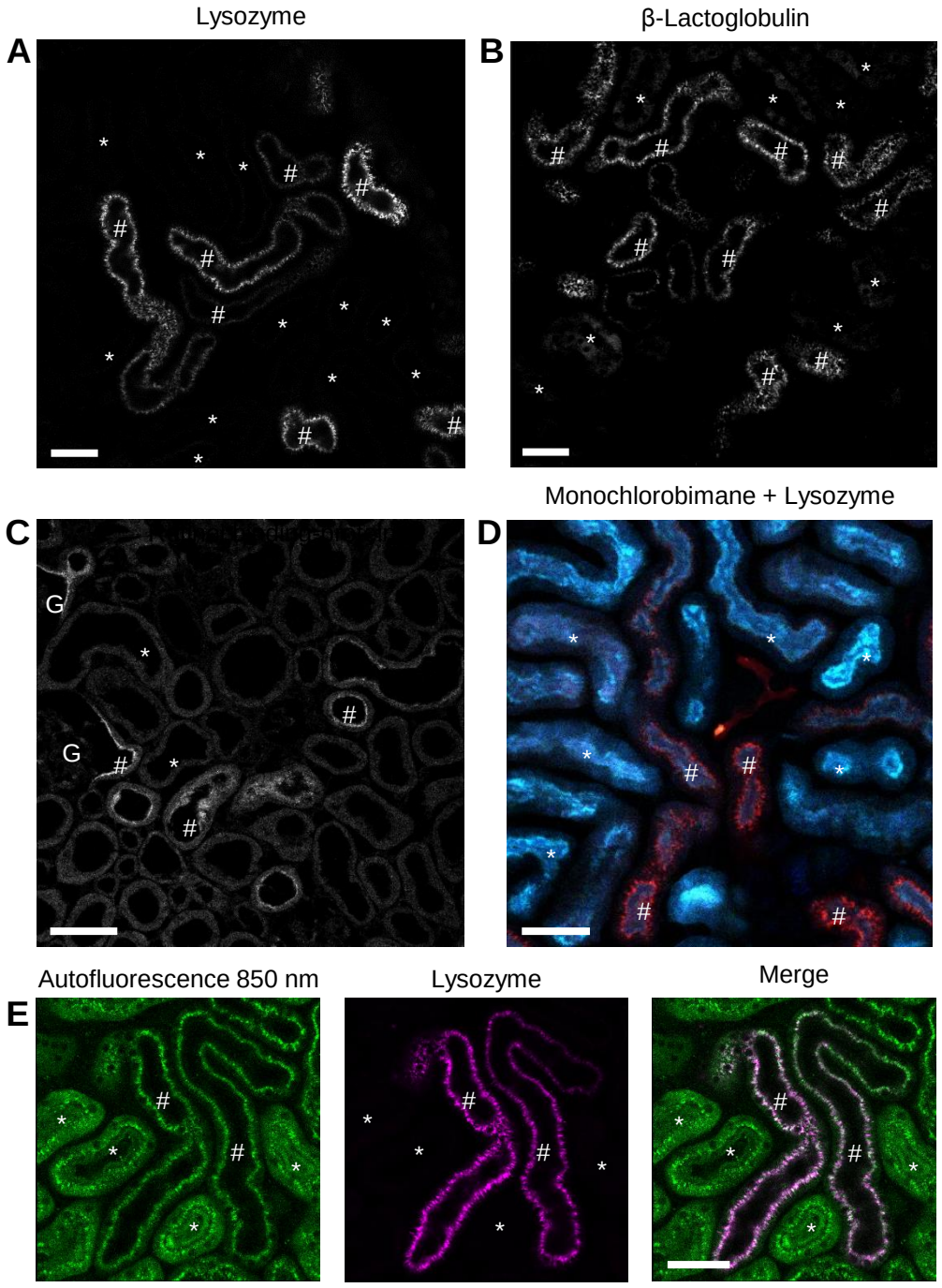

Figure S4: Low molecular weight protein reabsorption in the proximal tubule. (A-B) Multiphoton intravital imaging of the two low molecular weight proteins lysozyme (14.3 kDa) and β-lactoglobulin (18.4 kDa), both labeled with Atto565, revealed a similar uptake pattern with reabsorption only in S1 (#), but not S2 (*) segments of proximal tubules (PTs). (C) Antibody staining for endogenous retinol binding-protein 4 (eRBP4) in fixed tissue also revealed uptake only in early PT segments. G: glomerulus. (D) Co-injection of lysozyme (red) and monochlorobimane (blue) showing increased transport of the latter in lysozyme negative segments (*), confirming their S2 identity. (E) S1 (#) and S2 (*) PT segments could also be distinguished by their characteristic auto-fluorescence patterns in the green range at 850nm excitation. Images depicted in (E) were derived from the sum of 10 images in a time series. Scale bars: 50µm.

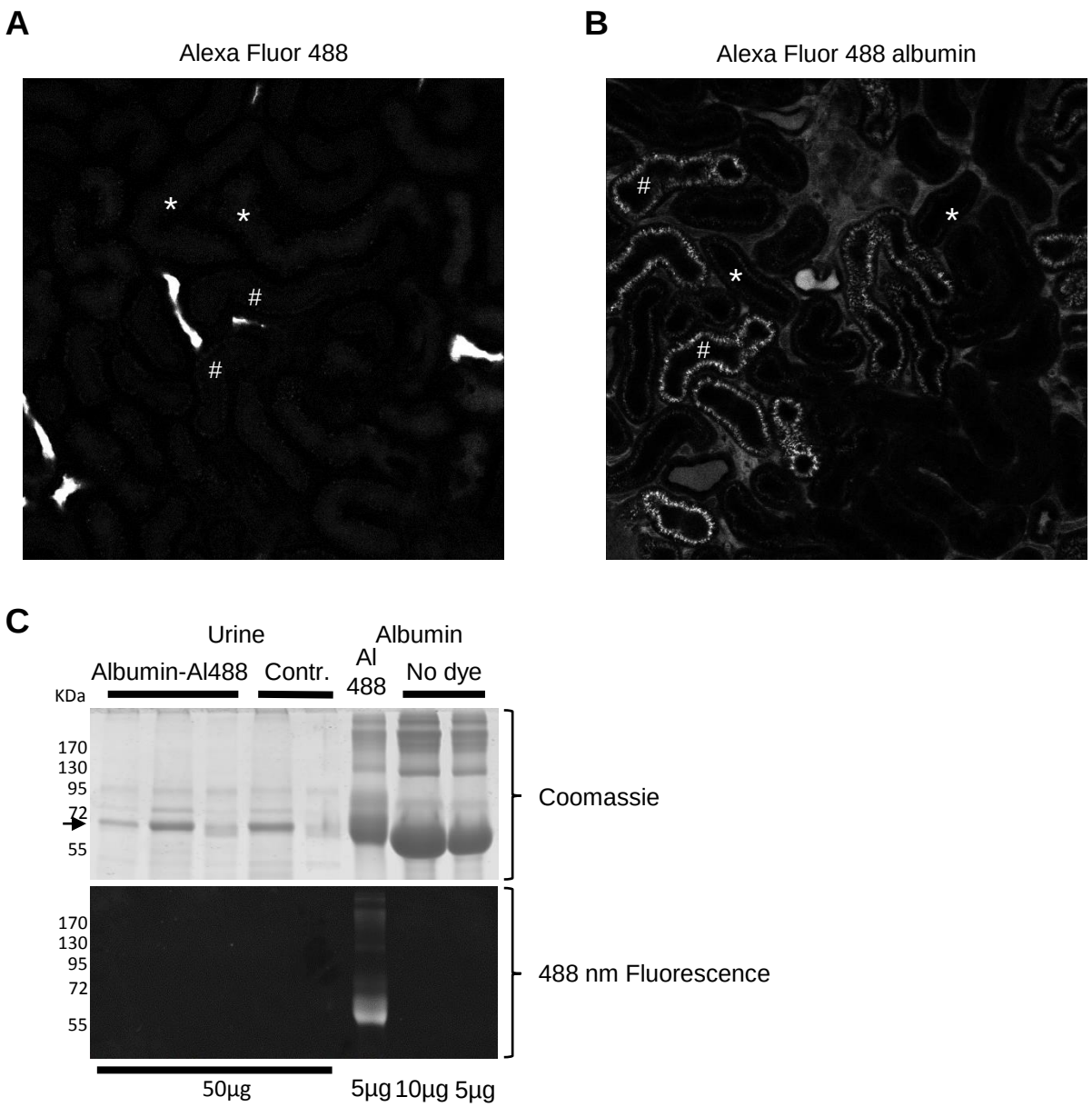

Figure S5: Comparison of free dye and labeled albumin uptake. (A-B) Multiphoton intravital imaging of intravenously injected free Alexa 488 dye (A) and Alexa 488-labeled albumin (B) revealed clearly different signal patterns. Labelled albumin was reabsorbed in S1 (#), but not S2 (*) segments of proximal tubules. In contrast, very little uptake of free dye was observed in S1 or S2 segments, and extensive wasting occurred in distal tubules. (C) Urine samples of 3 Alexa 488-labeled albumin injected mice and 2 control mice were separated by SDS-PAGE. 50µg of protein from the urine samples was loaded, and as a comparison albumin was directly loaded at different concentrations as indicated underneath. Only the directly loaded Alexa 488-labeled albumin gave a fluorescent signal, and this was not observed in any of the urine samples. However, a weak band for albumin (arrow) was found in all urine samples by Coomassie stain, consistent with urinary albumin excretion under physiological conditions, independent of albumin injection. Scale bars: 50µm.

Gene	Sense Primer	Antisense primer	Amplicons (bp)	Efficiency
Gapdh	TGCACCACCAACTGCTTAGC	GGATGCAGGGATGATGTTCT	176	1.02 ± 0.03
Sglt1	GTATGGTATGGTGGCCGATT	AATATCCAGCCCAGCACAAC	157	0.98 ± 0.03
Slc5a2	TTGGGCATCACCATGATTTA	GCTCCCAGGTATTTGTCGAA	164	0.94 ± 0.05
Car4	TGGCTCACTAACCACACCAA	GGCCTCACATTGTCCTTCAT	153	0.98 ± 0.03
Slc22a6	AAGCATGACTGCCGAGTTCT	CATCTGCTTCTGCTGTTCCA	190	0.95 ± 0.03
Slc22a8	GAGGAAGGGGAAAAGCTCAC	AACCAGGCCAGAGAGAGACA	154	1.01 ± 0.02
Slc22a19	CTGGAGATGCCCTAACCTTG	AAGCAGGCCCAATAAAGACA	173	1.01 ± 0.03
Rab7	GAGCGGACTTTCTGACCAAG	GGCAGTCACATCAAACACCA	152	0.99 ± 0.03
Lamp1	GAGTGGCAACTTCAGCAAGG	AGGCAGGTTCCGTTGTTACC	147	0.96 ± 0.03
Megalin	CAGTGGATTGGGTAGCAGGA	GCTTGGGGTCAACAACGATA	150	1.01 ± 0.02
Cubn	TCATTGGCCTCAGACATTCC	CCCAGACCTTCACAAAGCTG	149	0.99 ± 0.04

Supplementary table 1: Sequences of primers and efficiency of RT-PCR reactions.

Supplementary movie 1: Z-stack of cleared kidney tissue spanning the entire cortex, from the capsule on left to the medulla on right, and showing the uptake of lysozyme (red) and dextran (green) in proximal tubules.

Supplementary movie 2 3-D imaging of lysozyme uptake in cleared kidney cortex tissue, showing striking morphological heterogeneity of individually segmented proximal tubules.